Factors influencing the growth behaviour of nanoporous anodic films on iron under galvanostatic anodizing

Y. Konno[a], E. Tsuji[a, b], P. Skeldon[c], G.E. Thompson[c], H. Habazaki[a,b,d*]

[a]Graduate School of Chemical Sciences and Engineering, Hokkaido University, Sapporo, Hokkaido 060-68628, Japan

[b]Division of Materials Chemistry and [d]Frontier Chemistry Center, Faculty of Engineering,

[c]Corrosion and Protection Centre, School of Materials, The University of Manchester, Manchester, M13 9PL, United Kingdom

*Corresponding author; Phone & Fax: +81-11-706-6575, e-mail: habazaki@eng.hokudai.ac.jp

Abstract

The growth behaviour of nanoporous anodic films on iron during galvanostatic anodizing in ethylene glycol electrolytes containing NH_4F and H_2O is examined at various current densities, H_2O concentrations in electrolytes and temperatures. The film morphology is mainly controlled by the formation voltage, regardless of anodizing conditions. Relatively regular cylindrical pores are formed at formation voltages less than 50 V, while rather disordered pores are formed above 100 V. The decrease in the H_2O concentration suppresses chemical dissolution of anodic films in addition to the increased growth efficiency, resulting in the formation of anodic films with a steady thickness of ~7 μm. The cell size of the anodic films depends upon the H_2O concentration as well as the formation voltage, but not upon the current density. Findings in this study will be useful for controlled growth of the anodic films on iron.

Keywords: iron, anodizing, porous anodic film, organic electrolyte

1. Introduction

Anodizing of aluminium to form self-organized porous anodic oxide layers has been widely used in industry for corrosion protection, wear resistance and colouring of

aluminium and its alloys for more than a half century. The formation of such self-organized porous anodic films has been extended recently to a range of valve metals, including niobium, tantalum, titanium, tungsten and zirconium, since a report in 1999 by Zwelling et al. on the formation of nanoporous anodic films on a titanium alloy in fluoride-containing electrolytes [1].

Anodizing of iron in aqueous electrolytes at high potentials results in the formation of soluble ferrate ions [2,3], such that it has been presumed that no porous anodic films could be formed on iron. However, recent reports disclosed that nanoporous and nanotubular anodic films were formed in ethylene glycol or glycerol electrolyte containing fluoride and H_2O [4-9]. The anodic films formed are mainly amorphous and highly contaminated with fluoride species, but are readily converted to nanoporous or nanotubular α-Fe_2O_3, which is of potential interest as a photoanode for water splitting [4,7,10], photoelectrocatalyst [11] and electrodes of electrochemical capacitors [12].

The morphology of anodic films on iron is dependent upon the anodizing conditions. Albu et al. have reported the necessity of 0.1 to 2 mol dm^{-3} H_2O for the growth of nanoporous oxide films in 0.1 mol dm^{-3} NH_4F-ethylene glycol electrolyte [5]. They also revealed the transition from a nanoporous to a nanotubular structure by

increasing the electrolyte temperature from 293 to 313 K. The importance of the anodizing potential and water content for the nanoporous-to-nanotubular transition was also reported by Rangaraju et al [9]. Conversely, LaTempa et al. have reported an increased growth rate of the nanotubular iron oxide films at raised electrolyte temperatures, with a reduced influence of anodizing voltage and water content [6]. Our previous study using relatively thin, sputter-deposited iron films revealed that the initial growth rate of the nanoporous anodic films during galvanostatic anodizing in ethylene glycol electrolyte containing NH_4F and H_2O increased with a decrease in the water content, due to suppression of oxygen generation. The reduction of water content also results in a marked increase of formation voltage to higher than 150 V, disordering of the porous structure and enrichment of fluoride species at the metal/film interface [8]. Although these several studies have been carried out recently on the formation and morphology of the anodic films on iron, the information is still limited to understand systematically the growth of the anodic films on iron and to control precisely the morphology of the anodic films.

In the present study, the influences of anodizing conditions, i.e. current density and electrolyte temperature, as well as H_2O concentration in the electrolyte, on the growth behaviour of the nanoporous anodic films on iron have been examined

systematically using high purity bulk iron specimens under galvanostatic conditions in ethylene glycol electrolyte containing 0.1 mol dm^{-3} NH_4F and various concentrations of H_2O. By changing these three anodizing conditions, main parameters influencing the morphology, growth rate, maximum thickness and composition of the anodic films have been examined. The film morphology and carbon incorporation from electrolyte are found to be controlled mainly by the formation voltage, while the growth rate per unit electric charge is dependent upon the H_2O concentration in electrolyte, not upon the current density and formation voltage.

2. Experimental Details

High purity iron foils with a purity of 99.99 mass% were used for anodizing. The specimens were usually degreased in acetone prior to anodizing, except for those for GDOES analysis, which were mirror-polished using alumina abrasive of 3 μm diameter. Anodizing was carried out galvanostatically at a constant current density of 10 to 100 A m^{-2} in ethylene glycol containing 0.1 mol dm^{-3} NH_4F and 0.3 to 3.5 mol dm^{-3} H_2O at different temperatures between 283 K and 303 K.

The surfaces and fracture-sections of the resultant anodic films were observed using a JEOL JSM–6500F field emission scanning electron microscope, operated at an accelerating voltage of 10 kV. Cross-sections of the anodized specimens were also

observed using a JEOL JEM-2000FX transmission electron microscope, operated at 200 kV. Electron transparent sections were prepared by ultramicrotomy.

Depth profile analyses of the anodic films were undertaken by glow discharge optical emission spectroscopy (GDOES) using a Jobin-Yvon 5000 RF instrument in a neon atmosphere of 900 Pa by applying an RF of 13.56 MHz and a power of 50 W. Light emissions of characteristic wavelengths were monitored throughout the analysis with a sampling time of 0.01 s to obtain depth profiles. The wavelengths of the spectral lines used were 385.991, 130.217, 165.701, 149.26 and 685.602 nm for iron, oxygen, carbon, nitrogen, and fluorine, respectively. The signals were detected from a circular area of approximately 4 mm diameter. FTIR measurements were performed by Jasco FTIR-350 spectrometer with an MCT detector.

3. Results

3.1. Influence of H_2O concentration in electrolyte

Figure 1 shows the voltage-time curves of the iron specimen during anodizing at a constant current density of 50 A m^{-2} in the electrolytes containing several concentrations of H_2O. At all the H_2O concentrations, a voltage surge of ~6 V is observed at the commencement of anodizing, mainly due to the resistivity of electrolyte.

The formation voltage then increases gradually to a relatively steady value, which increases with a decrease in the H_2O concentration. The steady formation voltage is below 35 V in the electrolytes containing 0.5 mol dm^{-3} or lower H_2O, while the voltage increases to above 170 V by reducing the H_2O concentration to 0.3 mol dm^{-3}. During anodizing, gas evolution, probably oxygen, was visible to the naked eye in the electrolytes containing high concentrations of H_2O, but it became less significant with reduction of the H_2O concentration. These findings are consistent with the previous study using the magnetron-sputtered iron films [8].

Regardless of the H_2O concentration, porous anodic films are formed in the range of the H_2O concentrations between 0.3 and 2.5 mol dm^{-3} (Fig. 2). The size of the nanopores on the film surface is ~30 nm for the films formed with 0.3 and 0.5 mol dm^{-3} H_2O; further, the presence of rolling marks on the film surfaces suggests that no significant chemical dissolution of the anodic films occurs in these electrolytes (Figs. 2 (a, b)). In contrast, the surface of the nanoporous anodic film formed at 2.5 mol dm^{-3} H_2O (Fig. 2(c)) is relatively rough and no rolling marks are present, implying the occurrence of chemical dissolution of the anodic film. Thus, chemical dissolution of anodic films on iron appears to be accelerated by an increase in H_2O concentration. Further increase in the H_2O concentration to 3.5 mol dm^{-3} results in the development of

pits, as shown in Fig. 2(d). The presence of a certain amount of H_2O as well as fluoride ions may cause such local corrosive attack on iron.

Although the surface appearances of the anodic films formed at 0.3 and 0.5 mol dm^{-3} H_2O are similar (Figs. 2(a) and (b)), the cross-sectional morphologies differ as shown in Figs. 3(a) and (b). A disordered pore morphology is developed in the electrolyte containing 0.3 mol dm^{-3} H_2O (Fig. 3 (a)), while the film formed in the electrolyte containing 0.5 mol dm^{-3} H_2O has a relatively regular cylindrical pore morphology (Fig. 3(b)). At the higher H_2O concentration of 2.5 mol dm^{-3}, only a thin anodic film, 335 nm thick, is formed (Fig. 3(c)) as a consequence of enhanced gas generation and chemical dissolution of the anodic film during anodizing.

Figure 4 shows the change in film thickness as a function of anodizing time in the electrolytes containing different H_2O concentrations. The film thicknesses were measured by cross-sectional SEM observations. As reported previously [8], the film thickens linearly with anodizing time during initial anodizing time. The rate of film thickening increases with a reduction of the H_2O concentration in the electrolyte, due to reduced gas generation during anodizing. Then, the anodic films show a steady thickness with anodizing time, which is greater in the electrolytes with lower H_2O concentrations. In the electrolyte containing 0.3 mol dm^{-3} H_2O, uniform anodic films

were no longer formed when the anodizing time was extended beyond 1.8 ks, because of local detachment of the anodic film from the iron substrate. Thus, the thickest anodic film of 7.2 μm was obtained at a water concentration of 0.5 mol dm^{-3} H_2O after anodizing for 5.4 ks or longer. The large influence of H_2O concentration on the steady film thickness reveals the highly enhanced chemical dissolution at increased H_2O concentrations. As a consequence of chemical dissolution, even in the electrolyte containing 0.5 mol dm^{-3} H_2O, the pore size increases from 30 nm at anodizing time of 1.8 ks (Fig. 2 (b)) to 65 nm at the anodizing time of 7.2 ks (Fig. 5 (a)). The pore wall at the outer part of the anodic film formed at anodizing time of 7.2 ks (Fig. 5 (b)) also appears to be thinner than that near the base of the porous film (Fig. 5 (c)).

The film composition and phase structure may be dependent upon the H_2O concentration in electrolyte, such that the rate of film thickening increases and the gas generation is suppressed with a decrease in the H_2O concentration. The previous TEM observations of the anodic films disclosed that nanocrystals were present in the anodic films formed at higher H_2O concentrations while the anodic films were fully amorphous at reduced H_2O concentrations [8]. The nanocrystals may be probable sites of gas generation, as in the case of anodic TiO_2 [13,14], resulting in the enhanced gas generation at higher H_2O concentrations. GDOES depth profiles of the anodic films

revealed the incorporation of fluorine and carbon species from electrolyte. Figure 6 (a) is an example of the depth profile of the anodic film formed in the electrolyte containing 0.3 mol dm^{-3} H_2O. Fluorine, carbon and hydrogen species as well as oxygen are present throughout the film thickness. The FTIR spectrum of the anodized iron specimen revealed the absence of a C-H stretching vibration peak, while peaks were observed at 1373 and 1575 cm^{-1}, which suggested the presence of carbonate species. Thus, the carbon species incorporated into the anodic film do not have C-H bonds, and ethylene glycol may be oxidatively converted into carbonate species upon incorporation into the anodic film. In the depth profile, the decrease of the fluorine intensity near the metal/film interface is delayed in comparison with the oxygen intensity. Fluoride should enrich in the anodic film immediately above the metal substrate. The enrichment should be associated with the faster migration of fluoride ions, relative to that of O^{2-} ions under the high electric field during film growth [15,16]. However, the enrichment was only obvious at lower H_2O concentrations, at which the formation voltage increased to higher than 100 V [8]. The H_2O concentration-dependent enrichment of fluoride may be related to the mechanism of porous film growth, i.e., either field-assisted dissolution [17] or field-assisted flow [18,19]. The precise understanding of the growth mechanism is the subject of further study.

From the GDOES depth profile analysis, it was found that the intensity ratios between iron, oxygen and fluorine in the anodic films were similar, regardless of the H_2O concentration in electrolyte. In contrast, the content of carbon species increased with a decrease in the H_2O concentration in electrolyte (Fig. 6 (b)). At lower H_2O concentrations in the electrolyte, the incorporation of carbon species derived from ethylene glycol into the anodic film is promoted, probably as a consequence of a reduced H_2O concentration at the pore base, since H_2O is the source of oxygen in anodic films in organic electrolytes [20].

3.2. Influence of current density

As shown in Fig. 1, the formation voltage increases to more than 150 V in the electrolyte containing 0.3 mol dm^{-3} H_2O at a current density of 50 A m^{-2}. However, the formation voltage changes largely with current density even at the same H_2O concentration (Fig. 7). The initial voltage rise terminates at lower formation voltages when the current density is reduced. Steady voltages, 16 and 34 V, are achieved within the anodizing time of 300 s at current densities of 10 and 20 A m^{-2} respectively. The voltage-time response at 10 and 20 A m^{-2} is similar to that at 50 A m^{-2} in the electrolyte containing 2.5 and 0.5 mol dm^{-3} H_2O respectively. Thus, the voltage-time responses are

controlled by both H_2O concentration in electrolyte and current density.

The cross-sectional morphology of the anodic film formed at 20 A m^{-2} in the electrolyte containing 0.3 mol dm^{-3} H_2O (Fig. 8(a)) reveals the development of relatively regular cylindrical pores, which resemble the pore structure formed at 50 A m^{-2} in the electrolyte containing 0.5 mol dm^{-3} H_2O (Fig. 2(b)). When the current density increased to 100 A m^{-2} in the electrolyte containing 0.5 mol dm^{-3} H_2O, the formation voltage rose to ~150 V and an irregular pore structure, similar to that in Fig. 2(a), was developed. The findings suggest that the pore morphology is mainly controlled by the formation voltage and not directly by the H_2O concentration and current density.

Figure 8 (b) reveals a transmission electron micrograph of an ultramicrotomed section of the iron specimen anodized at 20 A m^{-2} in the electrolyte containing 0.3 mol dm^{-3} H_2O for 625 ks. The anodic film of ~350 nm thickness is amorphous, which is also evident from the halo in the selected area electron diffraction pattern shown in the inset of Fig. 8(b). When the anodic film was formed in the electrolyte containing higher H_2O concentrations, nanocrystals were present in the anodic film, even though the formation voltage was similar to that of the film shown in Fig. 9(b). Thus, it is suggested that the presence of nanocrystals is associated with the H_2O concentration in electrolyte, not with the formation voltage.

Probably associated with the formation of nanocrystals in the anodic films on iron, the growth rates of the anodic films are dependent upon the H_2O concentration in electrolyte [8]. Figure 9 shows the change in the thickness of anodic film with the charge passed during anodizing. At all conditions, the anodic films thicken linearly with the charge passed during anodizing up to 90 kC m^{-2}. Obviously, the slope is independent of the current density in galvanostatic anodizing, although the slope becomes lower with an increase in the water content of the electrolyte. Thus, the growth efficiency seems to be independent of the current density.

GDOES depth profile analyses have been carried out for the specimens anodized at several current densities in the electrolyte containing 0.3 mol dm^{-3} H_2O. The profiles were similar to that shown in Fig. 6(a), but the content of carbon species was dependent upon the current density (Fig. 10(a)). The intensity of carbon relative to that of iron in the anodic films increases with an increase in the current density. At high current densities, the film growth rate per unit anodizing time is enhanced. Thus, the H_2O concentration at the pore base should be reduced by the consumption of H_2O due to the formation of anodic films. As a consequence, the incorporation of carbon species into the anodic films is enhanced as in the case of the reduction of H_2O concentration in electrolyte. The relative intensity of carbon is re-plotted as a function of the final

formation voltage (Fig. 10(b)). In this figure, the data obtained at a current density of 50 A m^{-2} in the electrolytes with several H_2O concentrations are also plotted (solid circle). In both cases the relative carbon intensity increases with the formation voltage and interestingly, similar relative carbon intensities are obtained at similar formation voltages. Thus, the incorporation of carbon species is apparently controlled by the formation voltage. In contrast, the growth rate per unit electric charge is not dependent upon the formation voltage at the same H_2O concentration in electrolyte, as is evident from Figs. 7 and 9. Evidently, the content of incorporated carbon species in the anodic films does not affect the growth efficiency. As discussed above, the crystallinity of the anodic films influence the growth efficiency. The independency of the growth efficiency on the content of carbon species suggests that the carbon incorporation is not the critical factors influencing the nucleation of nanocrystals in the anodic films.

3.3. Influence of electrolyte temperature

Figure 11 shows the voltage-time curves of iron during anodizing at 50 A m^{-2} in the electrolyte containing 0.5 mol dm^{-3} H_2O for 1.8 ks at three different temperatures. The formation voltage increases gradually to ~250 V at the lowest temperature of 283 K, while steady voltages are obtained within 300 s at higher temperatures with the voltage

reducing with an increase in the temperature. After anodizing for 1.8 ks, the surfaces of the anodic films formed at and below 293 K were similar to those in Figs. 2(a) and (b), revealing no obvious chemical dissolution of the initially formed anodic films. The chemical dissolution of the anodic film appeared to be accelerated at 303 K, such that the film surface became slightly rough, similar to that shown in Fig. 5(a).

Cross-sectional scanning electron micrographs of the anodic film formed at 283 K (Fig. 12(a)) reveals a disordered pore morphology due to the increased formation voltage. Relatively regular cylindrical pores are developed at 293 K (Fig. 12(b)), at which the steady formation voltage is 35 V. Due to further decrease in the steady formation voltage at 303 K, the cell structure becomes finer (Fig. 12(c)).

4. Discussion

In our previous study [8], we found that the formation voltage changes largely with the H_2O concentration in electrolyte. At H_2O concentrations less than 0.5 mol dm^{-3}, the formation voltage increased to above 150 V at a current density of 50 A m^{-2} and the anodic films with highly disordered pore morphology was developed. The present study reveals that the formation voltages are controlled also by current density and electrolyte temperature. Thus, even at H_2O concentrations less than 0.5 mol dm^{-3}, the formation

voltages are reduced to less than 50 V, and relatively regular cylindrical pores are formed.

The growth rate of the anodic films is higher at lower H_2O concentrations, due to suppression of gas generation [8]. The present study also reveals that chemical dissolution is also suppressed by the reduction of H_2O concentration in electrolyte. Because of chemical dissolution, initial linear thickening of the anodic films with anodizing time is terminated at certain time of anodizing and the anodic films show a steady thickness. The steady thickness increases with a decrease in the H_2O concentration and the anodic films as thick as ~7 μm are formed at 0.5 mol dm^{-3} H_2O.

Regardless of the current density, H_2O concentration and electrolyte temperature, the morphology of the anodic films are mainly controlled by the formation voltage. When the formation voltage exceeds 100 V, disordered pores are always developed, while relatively regular cylindrical pores are formed below 50 V. It is well known that highly ordered pore arrays are formed at a particular formation voltage during anodizing of aluminium in aqueous acid electrolytes, i.e., 25 V in sulphuric acid [21], 40 V in oxalic acid [22] and 195 V in phosphoric acid [23]. In the present organic electrolytes, an optimized formation voltage appears to be present for the growth the ordered porous films, which should be between 30 and 50 V. The mechanism of

self-ordering of pores in porous anodic films on metals is not yet understood and is the subject of further studies, although some models, including a stress-induced flow of film materials from a pore base to a pore wall, have recently been proposed [18,24-26].

It is well known that the cell size of the anodic films on aluminium formed in acid aqueous electrolytes increases linearly with formation voltage [27,28]. In the present anodic films on iron, the cell sizes obtained at different current densities and electrolyte temperatures are plotted as a function of the steady-state formation voltage (Fig. 13). Obviously, at each H_2O concentration in the electrolyte, the cell size changes linearly with the formation voltage, similar to anodic alumina films. However, the cell size is also dependent upon the H_2O concentration in the electrolyte; a larger cell is developed at higher H_2O concentration at an identical formation voltage. At 1.5 mol dm^{-3} H_2O concentration, anodic films containing nanocrystals in an amorphous matrix are developed [8], while the anodic films are amorphous at 0.3 mol dm^{-3} H_2O concentration (Fig. 8(b)). Such film crystallization may contribute to the influence of H_2O concentration on the cell size. Conversely, the voltage-dependent incorporation of carbon species (Fig. 10(b)) has little influence on the cell size of the porous anodic films on iron.

Fig. 10(b) shows that the incorporation of carbon species into the anodic films

is apparently controlled by the formation voltage. However, the critical factors influencing the carbon incorporation should be the H_2O concentration at the pore bases and the electric field strength in the barrier layer. The H_2O concentration at the pore bases must be different from that of the bulk electrolyte, but the decrease in the H_2O concentration in electrolyte may reduce that at the pore bases. Then, the incorporation of the carbon species derived from ethylene glycol may be enhanced by lowering the H_2O concentration at the pore base. The reduction of H_2O concentration also leads to an increase in the formation voltage. Thus, both the formation voltage and carbon content increase with a decrease in the H_2O concentration. When the current density is increased, the consumption rate of H_2O at the pore bases for film formation must be increased together with the increase in the formation voltage. Thus, a positive correlation between the carbon incorporation and formation voltage is obtained when the current density is changed. The electric field strength also increases with the current density. It is known that incorporation of electrolyte species into anodic tantala is enhanced at higher field strength [29]. Thus, in the growth of porous anodic films on iron an increase in the electric field strength by increased current density may have some contribution to the enhanced incorporation of carbon species. The incorporated carbon species may also change the electric field in the barrier layer. However, the voltage-dependent

incorporation of the carbon species did not alter the linear correlation between the cell size and the formation voltage. Since the cell size is controlled by the thickness of the barrier layer, the results obtained suggest that the voltage-dependent incorporation of the carbon species has little influence on the electric field in the barrier layer.

5. Conclusions

In summary, the present study demonstrates that the formation voltage during galvanostatic anodizing of iron in ethylene glycol electrolytes containing NH_4F and H_2O is largely dependent upon the anodizing conditions, such as current density, H_2O concentration in electrolyte and electrolyte temperature. However, the morphology of the anodic films is mainly controlled by the formation voltage, regardless of the anodizing conditions. relatively regular cylindrical pores are formed below 50 V. Chemical dissolution of the anodic films is involved during anodizing, with the dissolution rate enhanced at higher H_2O concentration. Because of the reduced chemical dissolution and increased growth rate at lower H_2O concentrations, anodic films with a higher steady thickness (~7 μm) can be formed at 0.5 mol dm^{-3} H_2O. The cell size of the anodic films changes linearly with the formation voltage, as in the case of anodic alumina formed in aqueous acid electrolytes, but is also dependent upon the H_2O

concentration in electrolyte, probably associated with the H_2O concentration-dependent crystallization of the anodic films. Carbon species are incorporated into the anodic films, together with the fluoride species, with the carbon content increasing with the formation voltage. However, the voltage-dependent incorporation of carbon species does not influence the growth efficiency, cell size and crystallization of the anodic films.

Acknowledgments

This work was supported in part from the Advanced Technology Research Laboratories, Nippon Steel Corporation.

References

1. Zwilling V, Darque-Ceretti E, Boutry-Forveille A, David D, Perrin MY, Aucouturier M (1999) Structure and physicochemistry of anodic oxide films on titanium and Ta6V alloy. Surf Interface Anal 27 (7):629-637

2. Beck F, Kaus R, Oberst M (1985) Transpassive dissolution of iron to ferrate (VI) in concentrated alkali hydroxide solutions. Electrochim Acta 30 (2):173-183.

3. Pourbaix M (1974) Atlas of electrochemical equilibria in aqueous solutions. NACE, Houston

4. Prakasam HE, Varghese OK, Paulose M, Mor GK, Grimes CA (2006) Synthesis and

photoelectrochemical properties of nanoporous iron (III) oxide by potentiostatic anodization. Nanotechnol 17 (17):4285-4291

5. Albu SP, Ghicov A, Schmuki P (2009) High aspect ratio, self-ordered iron oxide nanopores formed by anodization of fe in ethylene glycol/NH_4F electrolytes. Physica Status Solidi-Rapid Res. Let. 3 (2-3):64-66

6. LaTempa TJ, Feng XJ, Paulose M, Grimes CA (2009) Temperature-dependent growth of self-assembled hematite (α-Fe_2O_3) nanotube arrays: Rapid electrochemical synthesis and photoelectrochemical properties. J Phys Chem C 113 (36):16293-16298

7. Rangaraju RR, Panday A, Raja KS, Misra M (2009) Nanostructured anodic iron oxide film as photoanode for water oxidation. J Phys D: Appl Phys 42 (13):135303

8. Habazaki H, Konno Y, Aoki Y, Skeldon P, Thompson GE (2010) Galvanostatic growth of nanoporous anodic films on iron in ammonium fluoride-ethylene glycol electrolytes with different water contents. J Phys Chem C 114 (44):18853-18859

9. Rangaraju RR, Raja KS, Panday A, Misra M (2010) An investigation on room temperature synthesis of vertically oriented arrays of iron oxide nanotubes by anodization of iron. Electrochim Acta 55 (3):785-793

10. Mohapatra SK, John SE, Banerjee S, Misra M (2009) Water photooxidation by smooth and ultrathin α-Fe_2O_3 nanotube arrays. Chem Mater 21 (14):3048-3055

11. Zhang ZH, Hossain MF, Takahashi T (2010) Self-assembled hematite (α-Fe_2O_3) nanotube arrays for photoelectrocatalytic degradation of azo dye under simulated solar light irradiation. Appl Cat B-Env 95 (3-4):423-429

12. Xie KY, Li J, Lai YQ, Lu W, Zhang ZA, Liu YX, Zhou LM, Huang HT (2011) Highly ordered iron oxide nanotube arrays as electrodes for electrochemical energy storage. Electrochem Commun 13 (6):657-660

13. Dyer CK, Leach JSL (1978) Breakdown and efficiency of anodic oxide growth on titanium. J Electrochem Soc 125:1032-1038

14. Habazaki H, Uozumi M, Konno H, Shimizu K, Skeldon P, Thompson GE (2003) Crystallization of anodic titania on titanium and its alloys. Corros Sci 45 (9):2063-2073

15. Shimizu K, Kobayashi K, Thompson GE, Skeldon P, Wood GC (1997) The migration of fluoride ions in growing anodic oxide films on tantalum. J Electrochem Soc 144 (2):418-423

16. Habazaki H, Fushimi K, Shimizu K, Skeldon P, Thompson GE (2007) Fast migration of fluoride ions in growing anodic titanium oxide. Electrochem Commun 9 (5):1222-1227

17. Garcia-Vergara SJ, Skeldon P, Thompson GE, Habazaki H (2007) A tracer investigation of chromic acid anodizing of aluminium. Surf Interface Anal 39 (11):860-864

18. Garcia-Vergara SJ, Skeldon P, Thompson GE, Habazaki H (2006) A flow model of porous anodic film growth on aluminium. Electrochim Acta 52 (2):681-687

19. Houser JE, Hebert KR (2009) The role of viscous flow of oxide in the growth of self-ordered porous anodic alumina films. Nat Mater 8 (5):415-420

20. Habazaki H, Oikawa Y, Fushimi K, Aoki Y, Shimizu K, Skeldon P, Thompson GE (2009) Importance of water content in formation of porous anodic niobium oxide films in hot phosphate-glycerol electrolyte. Electrochim Acta 54 (3):946-951

21. Masuda H, Hasegwa F, Ono S (1997) Self-ordering of cell arrangement of anodic porous alumina formed in sulfuric acid solution. J Electrochem Soc 144 (5):L127-L130

22. Masuda H, Fukuda K (1995) Ordered metal nanohole arrays made by a 2-step replication of honeycomb structures of anodic alumina. Science 268 (5216):1466-1468

23. Masuda H, Yada K, Osaka A (1998) Self-ordering of cell configuration of anodic porous alumina with large-size pores in phosphoric acid solution. Jpn J Appl Phys, Part 2-Let 37 (11A):L1340-L1342

24. Napolskii KS, Roslyakov IV, Eliseev AA, Byelov DV, Petukhov AV, Grigoryeva NA, Bouwman WG, Lukashin AV, Chumakov AP, Grigoriev SV (2011) The kinetics and mechanism of long-range pore ordering in anodic films on aluminum. J Phys Chem C 115 (48):23726-23731

25. Pashchanka M, Schneider JJ (2011) Origin of self-organisation in porous anodic alumina films derived from analogy with rayleigh-benard convection cells. J Mater Chem 21 (46):18761-18767

26. Hebert KR, Albu SP, Paramasivam I, Schmuki P (2012) Morphological instability leading to formation of porous anodic oxide films. Nat Mater 11 (2):162-166

27. O'Sullivan JP, Wood GC (1970) Morphology and mechanism of formation of porous anodic films on aluminum. Proc R Soc London, A 317:511-543

28. Ebihara K, Takahashi H, Nagayama M (1983) Structure and density of anodic oxide films formed on aluminum in oxalic acid solutions. J Surf Finish Soc Jpn 35 (4):548-553

29. Lu Q, Mato S, Skeldon P, Thompson GE, Masheder D, Habazaki H, Shimizu K (2002) Anodic film growth on tantalum in dilute phosphoric acid solution at 20 and 85ºC. Electrochim Acta 47 (17):2761-2767

Figure captions

Fig. 1 Voltage-time responses of iron during anodizing at a constant current density of 50 A m^{-2} in ethylene glycol electrolyte containing 0.1 mol dm^{-3} NH_4F and various concentrations of water at 293 K.

Fig. 2 Scanning electron micrographs of surfaces of the iron specimens anodized at a constant current density of 50 A m^{-2} in ethylene glycol electrolytes containing 0.1 mol L^{-1} NH_4F and (a) 0.3 mol dm^{-3}, (b) 0.5 mol dm^{-3}, (c) 2.5 mol dm^{-3} and (d) 3.5 mol dm^{-3} H_2O at 293 K for 1.8 ks.

Fig. 3 Cross-sectional scanning electron micrographs of the anodic films formed on iron at a constant current density of 50 A m^{-2} in ethylene glycol electrolytes containing 0.1 mol dm^{-3} NH_4F and (a) 0.3, (b) 0.5 and (c) 2.5 mol dm^{-3} H_2O at 293 K for 1.8 ks.

Fig. 4 Change in the thickness of the anodic films with anodizing time during anodizing of iron at a constant current density of 50 A m^{-2} in ethylene glycol electrolytes containing 0.1 mol dm^{-3} NH_4F and various concentrations of H_2O at 293 K.

Fig. 5 (a) Surface and cross-sections of the (b) outer and (c) inner parts of the anodic film formed on iron at a constant current density of 50 A m^{-2} in ethylene glycol electrolyte containing 0.1 mol dm^{-3} NH_4F and 0.5 mol dm^{-3} H_2O at 293 K for 7.2 ks.

Fig. 6 (a) GDOES depth profile of the anodic film formed on iron at a constant current density of 50 A m^{-2} in ethylene glycol electrolyte containing 0.1 mol dm^{-3} NH_4F and 0.3 mol dm^{-3} H_2O at 293 K for 250 s and (b) the intensity of carbon relative to that of iron in the anodic films as a function of H_2O concentration in electrolyte.

Fig. 7 Voltage-time responses of the iron specimen during anodizing at several current densities in ethylene glycol electrolyte containing 0.1 mol dm^{-3} NH_4F and 0.3 mol dm^{-3} H_2O at 293 K.

Fig. 8 Cross-sectional (a) scanning electron micrograph of the iron specimen anodized for 900s and (b) transmission electron micrograph of the iron specimen anodized for 625s at a constant current density of 20 A m^{-2} in ethylene glycol electrolyte containing 0.1 mol dm^{-3} NH_4F and 0.3 mol dm^{-3} H_2O at 293 K.

Fig. 9 Change in the thickness of the anodic films as a function of the electric charge passed during anodizing of iron at several current densities in the electrolytes containing 0.1 mol dm^{-3} NH_4F and 0.3 and 1.5 mol dm^{-3} H_2O at 293 K.

Fig. 10 (a) The GDOES intensity of carbon relative to that of iron in the anodic films formed in the electrolyte containing 0.1 mol dm^{-3} NH_4F and 0.3 mol dm^{-3} H_2O (a) a function of current density and (b) as a function of formation voltage. In (b), the data of the anodic films formed at 50 A m^{-2} in the electrolytes containing various H_2O concentrations are also included.

Fig. 11 Voltage-time responses of the iron specimen during anodizing at a constant current density of 50 A m^{-2} in ethylene glycol electrolyte containing 0.1 mol dm^{-3} NH_4F and 0.5 mol dm^{-3} H_2O at three different temperatures.

Fig. 12 Cross-sectional scanning electron micrographs of the anodic films formed on iron at a constant current density of 50 A m^{-2} in ethylene glycol electrolytes containing 0.1 mol dm^{-3} NH_4F and 0.5 mol dm^{-3} H_2O at (a) 283 K, (b) 293 K and (c) 303 K for 1.8 ks.

Fig. 13 Change in the average cell size of the anodic films formed on iron by galvanostatic anodizing in ethylene glycol electrolytes containing 0.1 mol dm^{-3} NH_4F and 0.3 and 1.5 mol dm^{-3} H_2O at various current densities and temperatures.

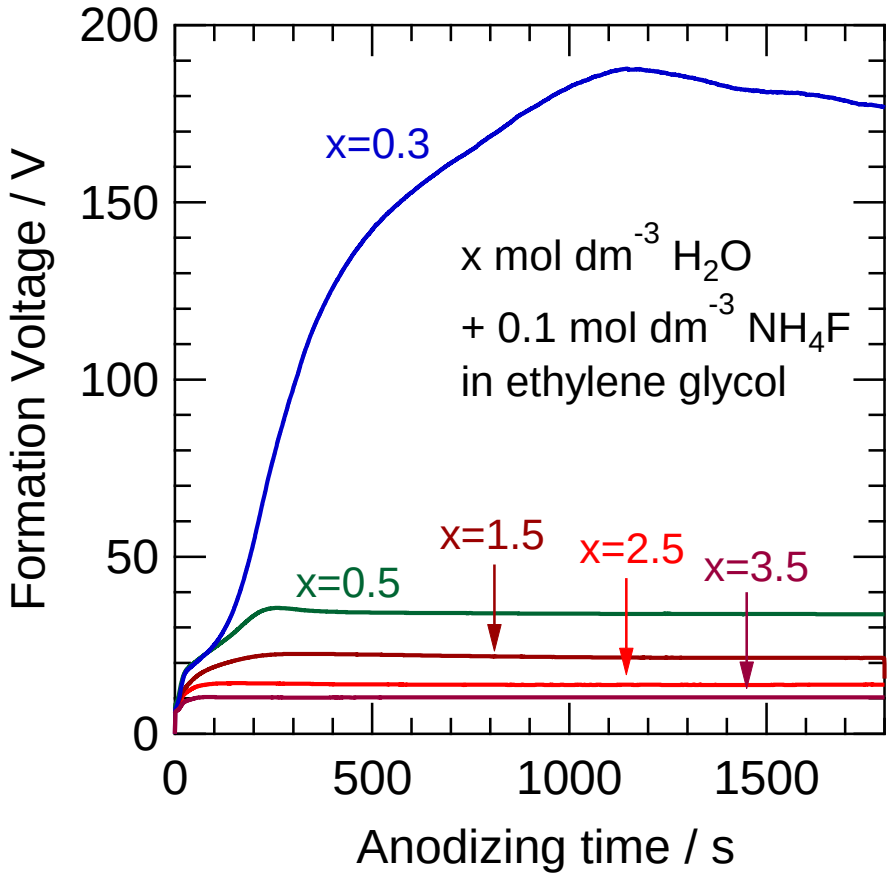

Fig. 1 Voltage-time responses of iron during anodizing at a constant current density of 50 A m^{-2} in ethylene glycol electrolyte containing 0.1 mol dm^{-3} NH_4F and various concentrations of water at 293 K.

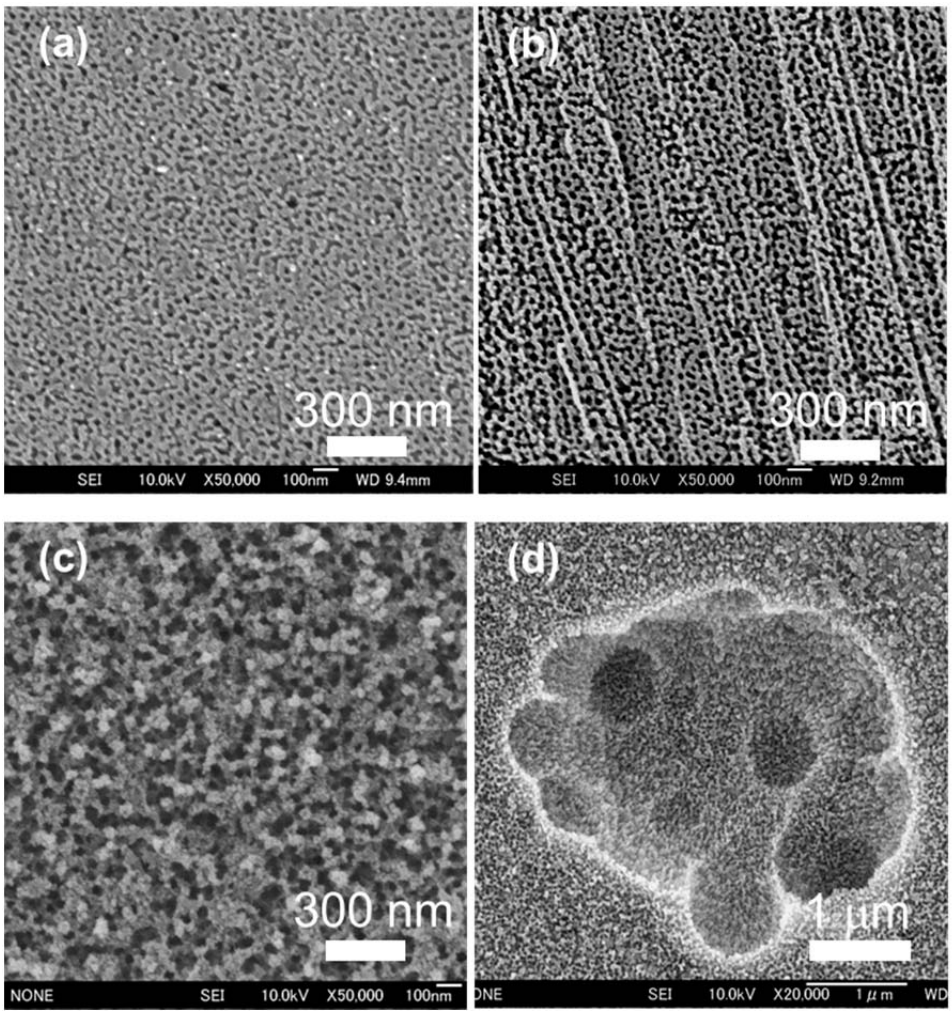

Fig. 2 Scanning electron micrographs of surfaces of the iron specimens anodized at a constant current density of 50 A m^{-2} in ethylene glycol electrolytes containing 0.1 mol L^{-1} NH_4F and (a) 0.3 mol dm^{-3}, (b) 0.5 mol dm^{-3}, (c) 2.5 mol dm^{-3} and (d) 3.5 mol dm^{-3} H_2O at 293 K for 1.8 ks.

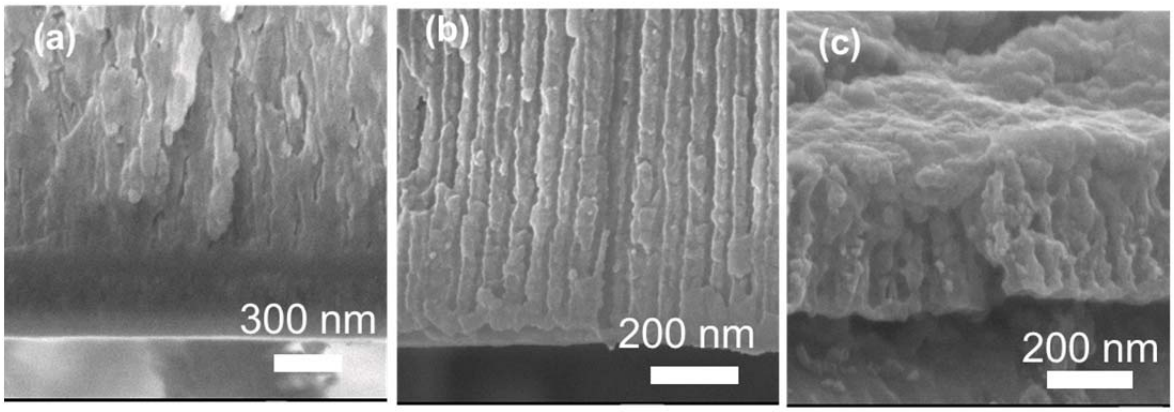

Fig. 3 Cross-sectional scanning electron micrographs of the anodic films formed on iron at a constant current density of 50 A m^{-2} in ethylene glycol electrolytes containing 0.1 mol dm^{-3} NH_4F and (a) 0.3, (b) 0.5 and (c) 2.5 mol dm^{-3} H_2O at 293 K for 1.8 ks.

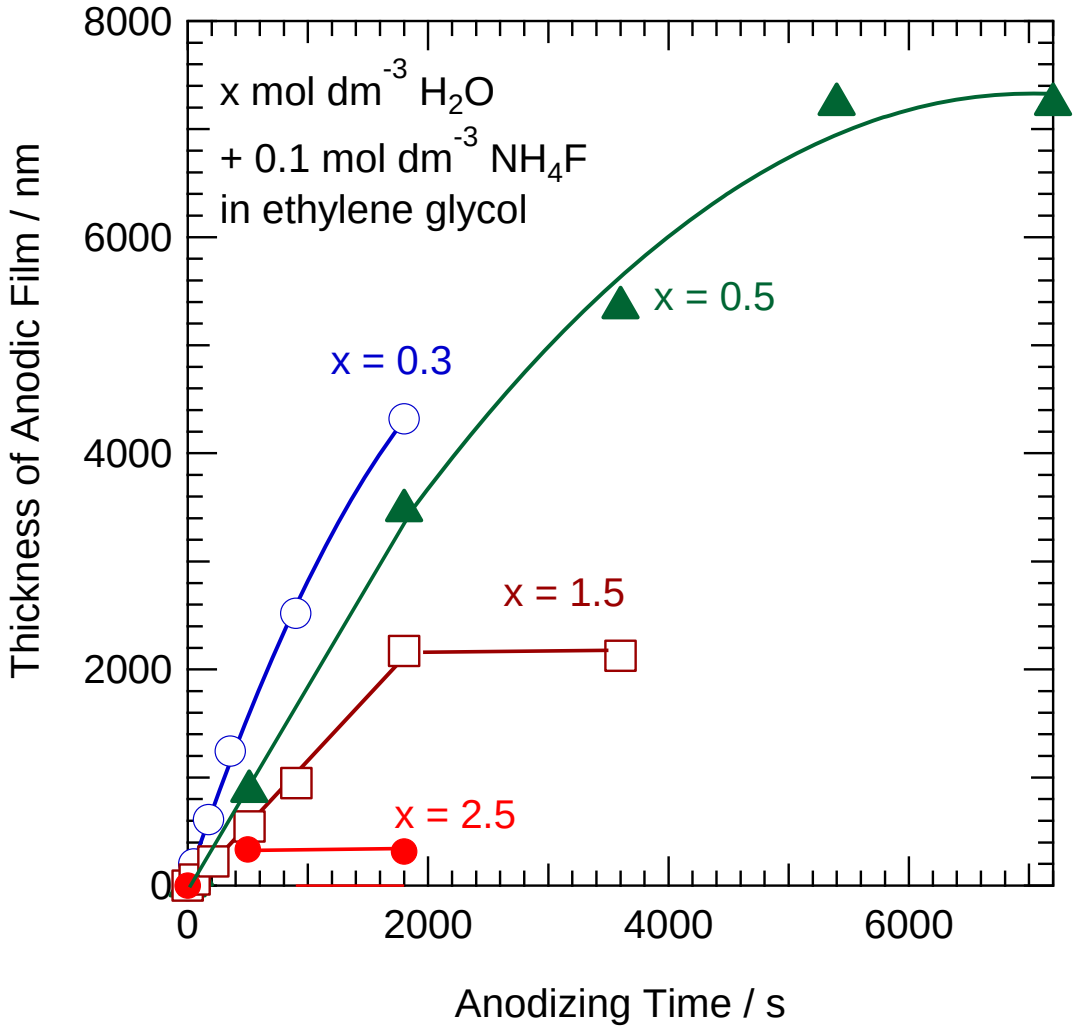

Fig. 4 Change in the thickness of the anodic films with anodizing time during anodizing of iron at a constant current density of 50 A m^{-2} in ethylene glycol electrolytes containing 0.1 mol dm^{-3} NH_4F and various concentrations of H_2O at 293 K.

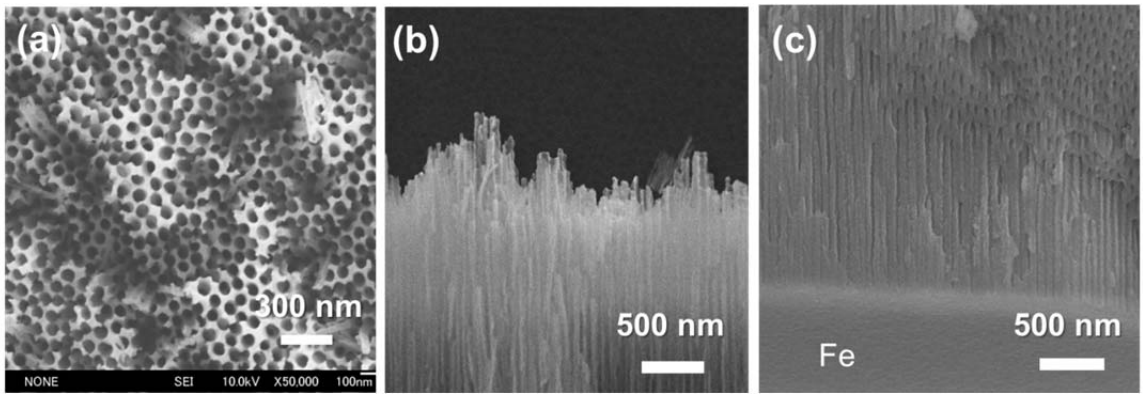

Fig. 5 (a) Surface and cross-sections of the (b) outer and (c) inner parts of the anodic film formed on iron at a constant current density of 50 A m^{-2} in ethylene glycol electrolyte containing 0.1 mol dm^{-3} NH_4F and 0.5 mol dm^{-3} H_2O at 293 K for 7.2 ks.

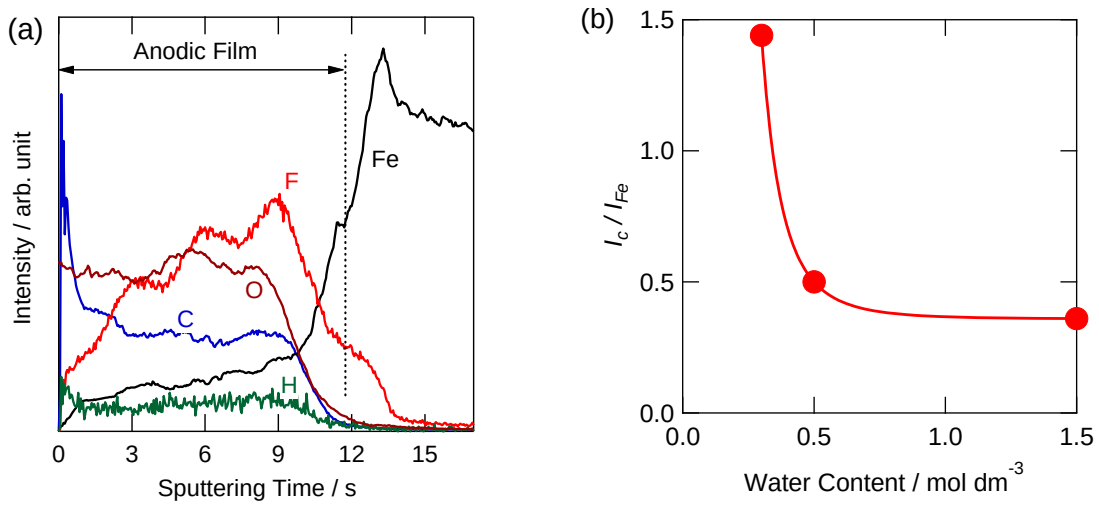

Fig. 6 (a) GDOES depth profile of the anodic film formed on iron at a constant current density of 50 A m^{-2} in ethylene glycol electrolyte containing 0.1 mol dm^{-3} NH_4F and 0.3 mol dm^{-3} H_2O at 293 K for 250 s and (b) the intensity of carbon relative to that of iron in the anodic films as a function of H_2O concentration in electrolyte.

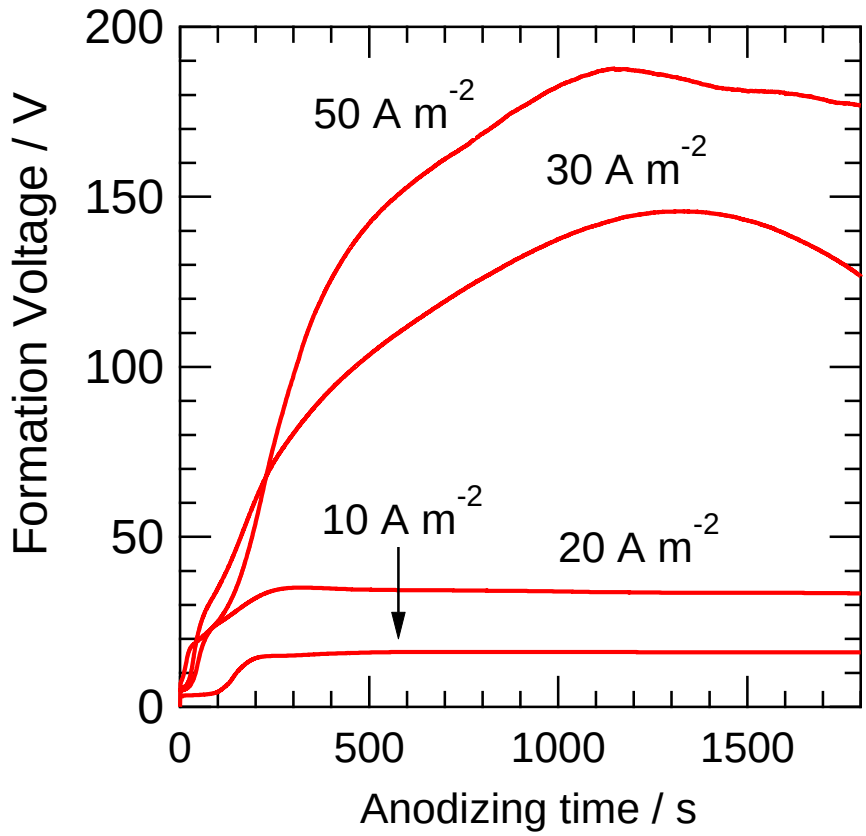

Fig. 7 Voltage-time responses of the iron specimen during anodizing at several current densities in ethylene glycol electrolyte containing 0.1 mol dm^{-3} NH_4F and 0.3 mol dm^{-3} H_2O at 293 K.

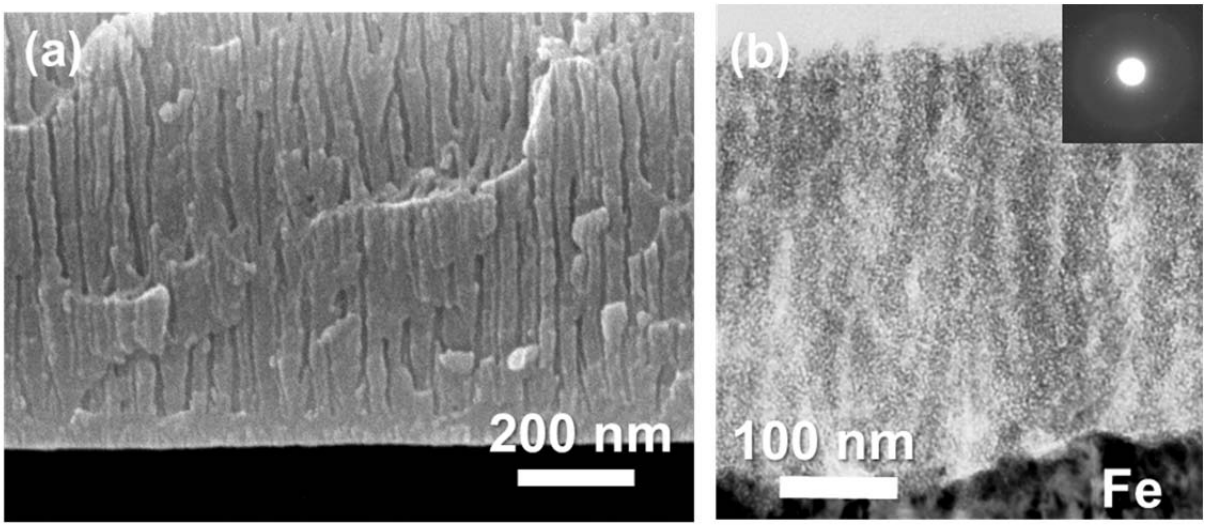

Fig. 8 Cross-sectional (a) scanning electron micrograph of the iron specimen anodized for 900s and (b) transmission electron micrograph of the iron specimen anodized for 625s at a constant current density of 20 A m^{-2} in ethylene glycol electrolyte containing 0.1 mol dm^{-3} NH_4F and 0.3 mol dm^{-3} H_2O at 293 K.

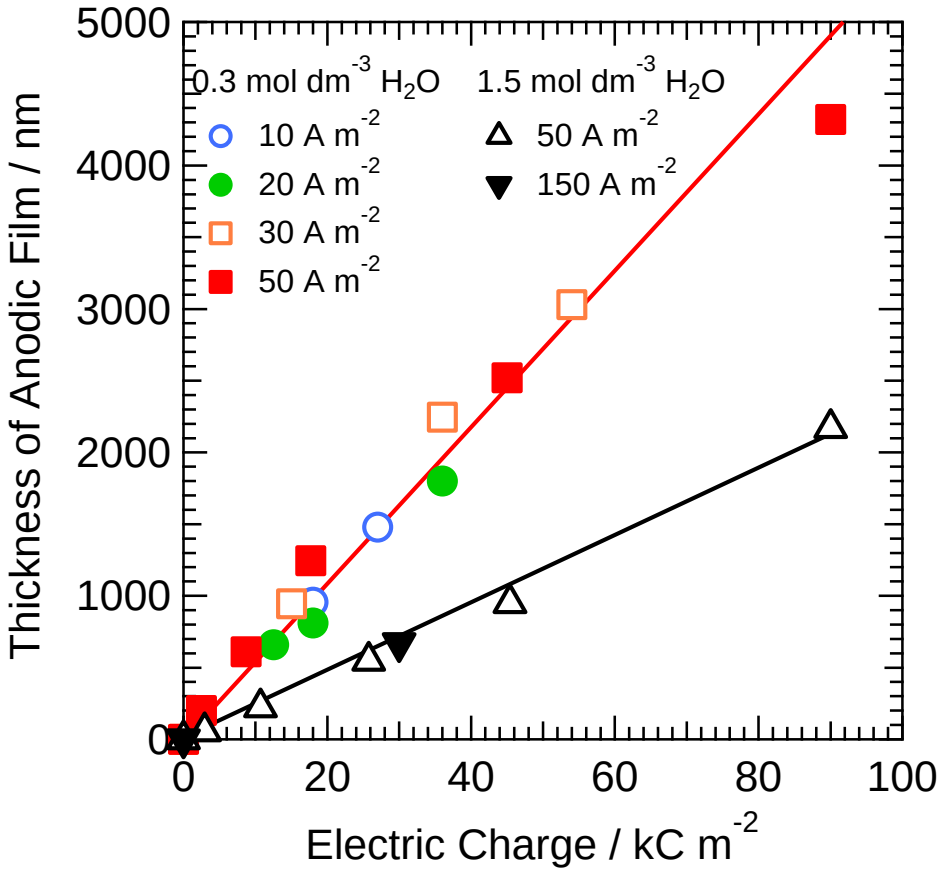

Fig. 9 Change in the thickness of the anodic films as a function of the electric charge passed during anodizing of iron at several current densities in the electrolytes containing 0.1 mol dm^{-3} NH_4F and 0.3 and 1.5 mol dm^{-3} H_2O at 293 K.

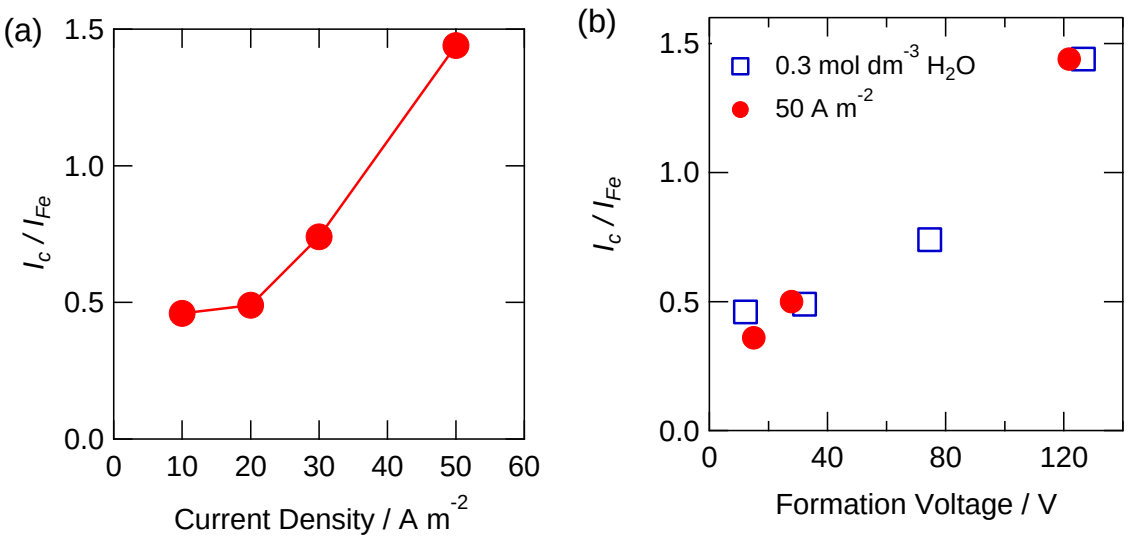

Fig. 10 (a) The GDOES intensity of carbon relative to that of iron in the anodic films formed in the electrolyte containing 0.1 mol dm^{-3} NH_4F and 0.3 mol dm^{-3} H_2O (a) a function of current density and (b) as a function of formation voltage. In (b), the data of the anodic films formed at 50 A m^{-2} in the electrolytes containing various H_2O concentrations are also included.

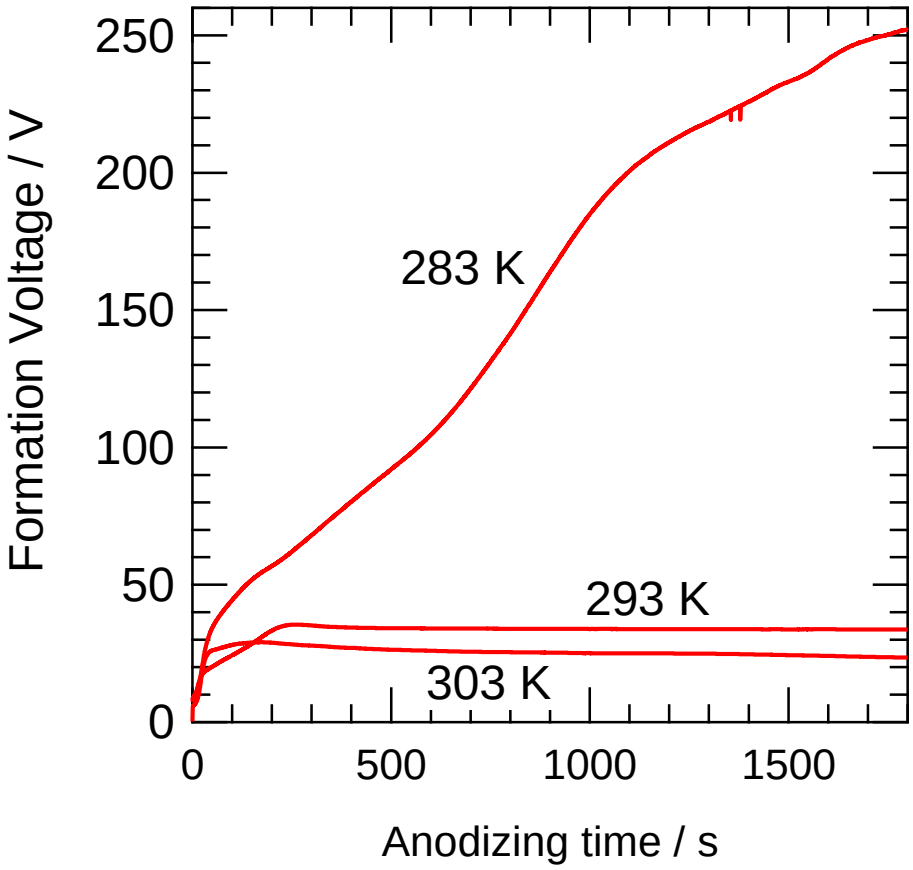

Fig. 11 Voltage-time responses of the iron specimen during anodizing at a constant current density of 50 A m^{-2} in ethylene glycol electrolyte containing 0.1 mol dm^{-3} NH_4F and 0.5 mol dm^{-3} H_2O at three different temperatures.

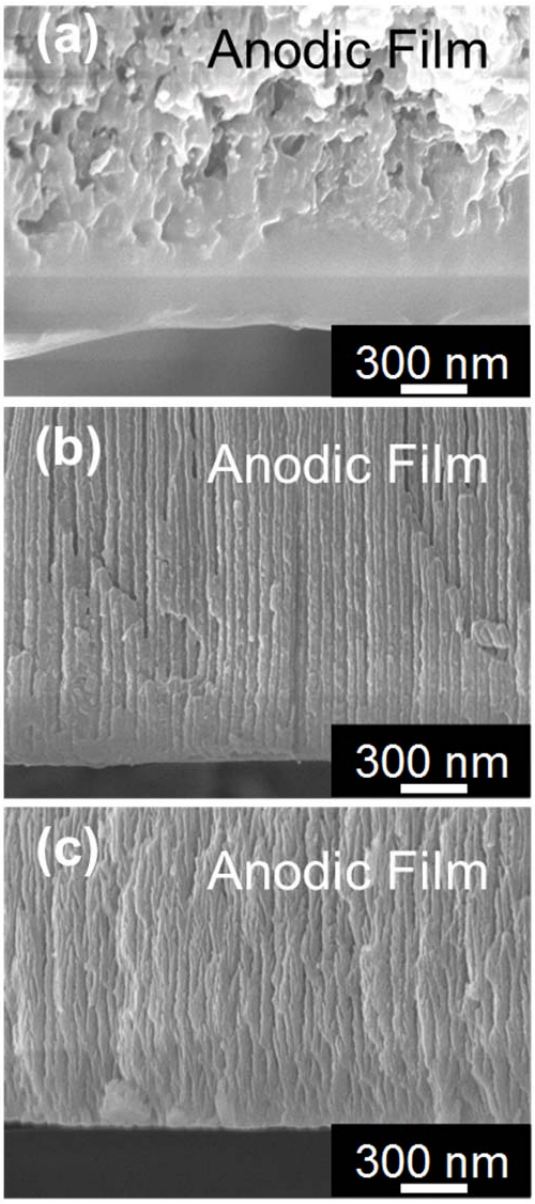

Fig. 12 Cross-sectional scanning electron micrographs of the anodic films formed on iron at a constant current density of 50 A m^{-2} in ethylene glycol electrolytes containing 0.1 mol dm^{-3} NH_4F and 0.5 mol dm^{-3} H_2O at (a) 283 K, (b) 293 K and (c) 303 K for 1.8 ks.

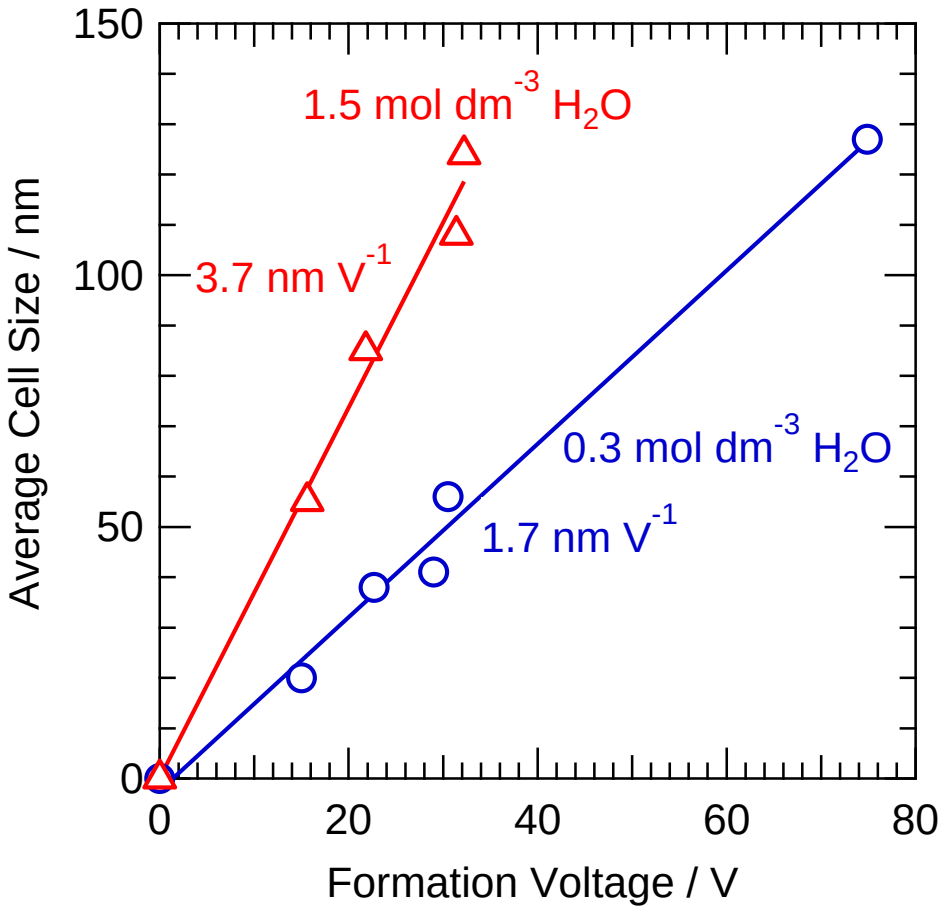

Fig. 13 Change in the average cell size of the anodic films formed on iron by galvanostatic anodizing in ethylene glycol electrolytes containing 0.1 mol dm^{-3} NH_4F and 0.3 and 1.5 mol dm^{-3} H_2O at various current densities and temperatures.